RESEARCH ARTICLE

Asymmetry-enhanced ^{59}Co NMR thermometry in Co(III) complexes†

Ökten Üngör, [ID] Stephanie Sanchez, Tyler M. Ozvat [ID] and Joseph M. Zadrozny [ID] *

Design strategies for molecular thermometers by magnetic resonance are essential for enabling new non-invasive means of temperature mapping for disease diagnoses and treatments. Herein we demonstrate a new design strategy for thermometry based on chemical control of the vibrational partition function. To do so, we performed variable-temperature ^{59}Co NMR investigations of four air-stable Co(III) complexes: Co(accp)$_3$ (**1**), Co(bzac)$_3$ (**2**), Co(tBu$_2$-acac)$_3$ (**3**), and Co(acac)$_3$ (**4**) (accp = 2-acetylcyclopentanonate; bzac = benzoylacetonate; tBu$_2$-acac = 2,2,6,6-tetramethyl-3,5-heptanedionate and acac = acetylacetonate). We discovered ^{59}Co chemical shift temperature sensitivity ($\Delta\delta/\Delta T$) values of 3.50(2), 3.39(3), 1.63(3), and 2.83(1) ppm °C^{-1} for **1**–**4**, respectively, at 100 mM concentration. The values observed for **1** and **2** are new records for sensitivity for low-spin Co(III) complexes. We propose that the observed heightened sensitivities for **1** and **2** are intimately tied to the asymmetry of the accp and bzac ligands *versus* the acac and tBu$_2$-acac ligands, which enables a larger number of low-energy Raman-active vibrational modes to contribute to the observed $\Delta\delta/\Delta T$ values.

Introduction

Thermometry by magnetic resonance imaging, which utilizes nuclear magnetic resonance (NMR) technology, is a powerful technique for noninvasive monitoring of temperature.[1–3] This capability is important in biomedical treatments, *e.g.* monitoring the progression of thermal ablation of tumors. Moreover, the technique is also important for simply achieving a deeper fundamental understanding of internal temperature regulation in the body, which is poorly understood and still yielding new insights to this day.[4] Designing molecular probes that enable high temperature/spatial resolution *in vivo* is an essential component of improving thermometer capabilities.

One method for temperature detection *via* NMR utilizes a temperature-dependent chemical shift. This technique can use protons (^{1}H),[5–7] ^{19}F,[8,9] ^{13}C,[10,11] and ^{31}P.[12,13] Yet, the temperature sensitivities of these systems are often low, <1 ppm °C^{-1} (*e.g*, 0.01 ppm °C^{-1} for ^{1}H in H$_2$O,[6] or 0.012 ppm °C^{-1} in ^{19}F as perfluorotributylamine[9]). A related technique, PARACEST (PARAmagnetic Chemical Exchange Saturation Transfer), can imbue a temperature dependence to the ^{1}H chemical shift of bulk water through hyperfine coupling in open-shell lanthanide complexes.[14,15] These strategies also generally produce temperature sensitivities of *ca.* 1 ppm °C^{-1}.

The ^{59}Co nucleus in low-spin Co(III) complexes is a particularly attractive alternative system for chemical-shift-based thermometry applications.[16] The ^{59}Co nucleus is 100% naturally abundant, exhibits a nuclear spin of $I = ^7/_2$, has a high receptivity (*ca.* 30% that of ^{1}H), and displays a wide reported chemical shift (δ) window (20 000 ppm), which reflects an exquisite sensitivity of δ to electronic structure and the ligand field splitting (Δ_o).[17,18] Importantly, the ^{59}Co nucleus also typically yields a large temperature-dependent chemical shift, $\Delta\delta/\Delta T$, of 1–3 ppm °C^{-1} in magnitude, which stems from the temperature dependence of Δ_o. In 1980, Levy and co-workers set the record for $\Delta\delta/\Delta T$ with Co(acac)$_3$ (acac = acetylacetonate), which displayed a 3.15 ppm °C^{-1} $\Delta\delta/\Delta T$ for the ^{59}Co nucleus.[19]

A target sensitivity of *ca.* 10 ppm °C^{-1} for ^{59}Co is ideal to balance the typical wide linewidths of the peaks, and the gradient range in an MRI scanner, and avoid the need for retuning the instrument mid-measurement. A molecule to reach this target parameter should ideally also be air stable to facilitate biomedical imaging applications. In light of these requirements, the recently reported[20] record (>100 ppm °C^{-1}) sensitivities in [(CpCo(OP(OR)$_2$)$_3$)$_2$]Co$^+$ (R = Me, Et, tBu) are too large. The complexes are also air sensitive, and these two properties together limit applicability. Separately, one complex that is closer to the 10 ppm °C^{-1} goal, [^{tBu}(PNP)Fe–H], exhibits thermal sensitivities of 14 ppm °C^{-1} (^{1}H)[21] and 34 ppm °C^{-1} (^{31}P)[22] though these molecules are also, unfortunately, air sensitive. Hence, design strategies to maximize $\Delta\delta/\Delta T$ in an air-

*Department of Chemistry, Colorado State University, Fort Collins, Colorado 80523, USA. E-mail: joe.zadrozny@colostate.edu*

7064 | *Inorg. Chem. Front.*, 2023, **10**, 7064–7072

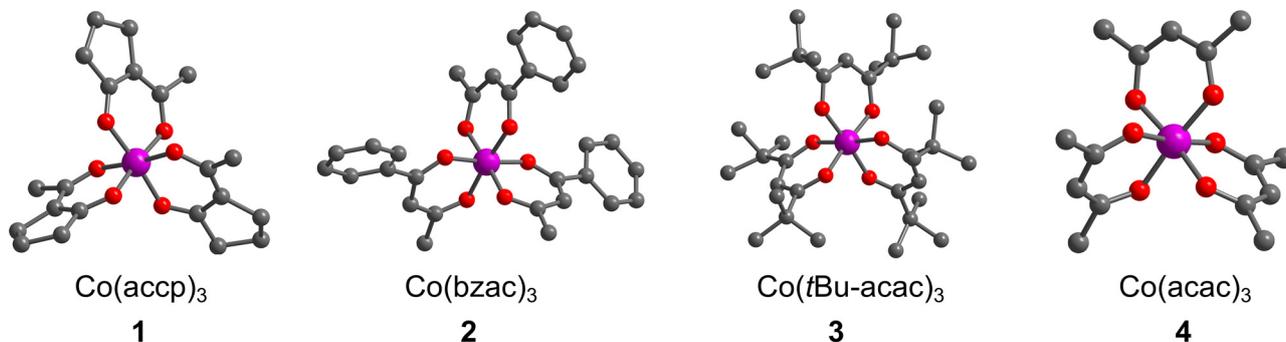This journal is © the Partner Organisations 2023

stable compound remains a key target of fundamental understanding.

We recently proposed a route to a higher $\Delta\delta/\Delta T$ through designing the vibrational partition function. In this strategy, the target parameter for higher $\Delta\delta/\Delta T$ is a larger number of low-energy symmetric (Raman-active) vibrational modes.[23] A group-theory analysis of the CoO_6 coordination shell of Co (acac)$_3$ reveals 15 possible vibrations, but local D_3 symmetry ensures that only 12 of these are Raman active (Fig. 1). We hypothesized that the 3 lost vibrations could be diminishing the partition function, and, hence, lowering $\Delta\delta/\Delta T$. We hypothesized that a system with asymmetric bidentate ligands would lower local point group symmetry to C_3 (or lower), symmetries where all vibrations are Raman active, and hence ensure a higher partition function and thus higher $\Delta\delta/\Delta T$.

Herein we report the synthesis and ^{59}Co NMR characterization of a set of Co(III) complexes with asymmetric analogues of the acac ligand: Co(accp)$_3$ (**1**, accp = 2-acetylcyclopentanonate), Co(bzac)$_3$ (**2**, bzac = benzoylacetonate), Co(tBu$_2$-acac)$_3$ (**3**, tBu$_2$-acac = 2,2,6,6-tetramethyl-3,5-heptanedionate) and Co (acac)$_3$ (**4**, acac = acetylacetonate), Fig. 2. We hypothesized that the ligands of **1** and **2** would enforce a higher $\Delta\delta/\Delta T$ than the original report of Co(acac)$_3$.[19] We show that this asymmetry-focused design strategy based on maximizing the vibrational partition function can indeed be harnessed to raise $\Delta\delta/\Delta T$.
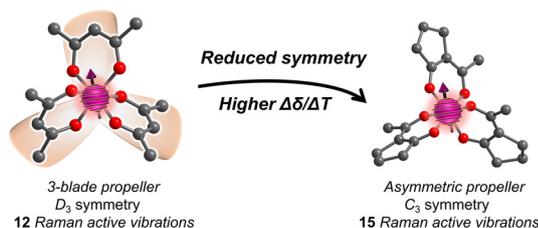
Fig. 1 The CoO_6 coordination geometry in D_3 symmetry (like a three-bladed propeller) has 15 possible vibrations, only 12 are active for temperature sensitivity. In contrast, the molecule on the right, with asymmetric ligands, could exploit all 15 for temperature sensitivity.

Results and discussion
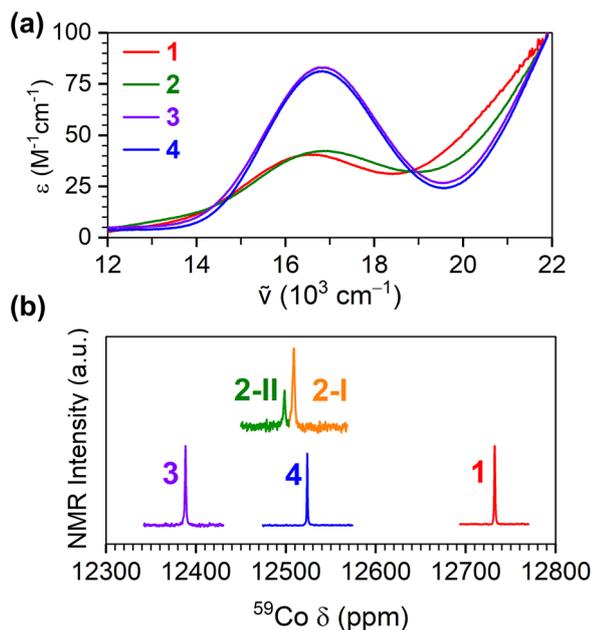
Syntheses and molecular structures

Compounds **1**–**4** are all pseudooctahedral, low-spin Co(III) complexes. Single crystals of **1** were grown by slow evaporation from acetonitrile (MeCN), and the structures of **2**–**4** were previously reported[24–26] – all are shown in Fig. 2. All complexes exhibit six-coordinate inner coordination shells with 6 donor O atoms. Average Co–O bond distances are 1.88(2) Å for **1**, which are in the range of reported average distances of 1.81(2), 1.86(1), and 1.90(2) for **2**–**4**. The average O–Co–O bite angle for **1** is 89.2(2)°, close to 90.04(13), 92.3(2), and 92.9(3)° for **2**–**4**, respectively. Continuous-shape-measurement analyses were also performed to check for geometric structural trends.[27,28] For an idealized octahedral O_h geometry, SHAPE scores are 0. The scores for **1**–**4** are 0.34, 0.28, 0.08 and 0.37, respectively, indicating that all four complexes closely resemble perfect octahedral geometry.

The ligands in **1**–**4** direct the molecular point group of the complex. In **3** and **4**, which have C_{2v}-symmetric acac and tBu$_2$-acac ligands, the local coordination environments of the Co(III) ions are D_3 symmetry. In contrast, **1** and **2**, which have asymmetric ligands, have two possible forms. If the ligands in these complexes are all oriented similarly, then local C_3 symmetry is possible, resulting in a *fac* isomer. If one of the ligands is flipped in orientation relative to the other two, the local symmetry is C_1 (the *mer* isomer). In the single-crystal diffraction data, only the *mer* isomer is observed for **1**. However, in the structure of **2** one of the bzac ligands is disordered and hence the *mer* and *fac* isomers are both present in the single crystal.[24]

Electronic structures. We first studied the electronic structures of the cobalt(III) ions in **1**–**4** by electronic absorption spectroscopy. UV-vis absorption spectra of compounds **1**–**4** measured in CH_2Cl_2 at room temperature (Fig. 3a and Fig. S1†) revealed two sets of absorption bands. Absorptions with molar absorptivity coefficients, ε, of *ca.* 30–80 M^{-1} cm^{-1} around 16 700 cm^{-1} (600 nm) give **1**–**4** deep green colors in solution, and these are likely d–d transitions, specifically the $^1A_{1g}$ to $^1T_{2g}$ transition.[29–31] All molecules also give more

Fig. 2 The crystal structures of the Co(III) complexes studied in this manuscript. Structures of **2**–**4** are taken from previous reports.[24–26] H atoms are omitted for clarity. Color scheme; Co: violet, O: red, C: gray.

This journal is © the Partner Organisations 2023

Inorg. Chem. Front., 2023, **10**, 7064–7072 | **7065**

Fig. 3 Characterization of Co(III) electronic structure in **1–4**. (a) UV-vis spectra for **1–4** in CH_2Cl_2 at room temperature, focused on the d–d transition. (b) [59]Co NMR spectra (*ca.* 118.3 MHz) for **1–4** in $CDCl_3$ at room temperature. Spectra were collected in a 500 MHz ^{1}H magnet (11.7 T).

intense (*ca.* 250 M^{-1} cm^{-1}) peaks at much higher energies; 29 000 and 30 600 cm^{-1} for **1** and **4**. These same high-energy transitions are very broad for **3**, spanning 28 571 to 33 333 cm^{-1}. Lastly, two transitions of this type are observed for **2** at 34 965 and 38 610 cm^{-1}. These high-energy transitions are likely ligand π–π^* transitions.[32]

The energies of the low-energy peaks and the d^6 Tanabe–Sugano diagram[33] allowed us to quantify Δ_o, which increases in order from **1** (16 502 cm^{-1}) to **4** (16 850 cm^{-1}) to **2** (16 852 cm^{-1}) to **3** (16 885 cm^{-1}). The value of **4** is consistent with the literature value,[29] whereas the values for the other three have not been previously reported. In all, these values suggest generally weak ligand fields for the Co(III) ions and control for the possibility of substantial ligand field differences causing the observed trends in $\Delta\delta/\Delta T$.

For all four complexes, the [59]Co NMR chemical shift varied within 12 400 to 12 800 ppm (Fig. 3b). These values are within the range of [59]Co NMR peaks of previously reported all-oxygen-bound octahedral Co(III) complexes.[16] An important feature of the [59]Co NMR spectra of **2** is the presence of two peaks. We note that prior DFT calculations and ^{1}H NMR analyses of **2** reveal both *fac* and *mer* isomers to be stable,[34] and disorder in the crystal structure of **2** indicates the presence of both isomers. We tentatively assign the two [59]Co NMR peaks to the respective isomers as **2-I** (for *mer*) and **2-II** (for *fac*). This assignment is based on literature references indicating that the *fac* isomer exhibits greater shielding, narrower linewidth and lower signal intensity.[34,35] We note that only one peak is observed for **1**, suggesting that only one isomer is present,

which is consistent with the lack of any disorder in the crystal structure. Finally, the known correlation of [59]Co chemical shifts to Δ_o[17] indicates the magnitude of Δ_o increases in the order of **1** < **4** < **2** < **3**, in agreement with the lowest-energy peak in the UV-vis data above.

We also conducted diffuse-reflectance spectroscopy (DRS) on these compounds for comparison between solution and solid-state electronic structures and, by proxy, physical structure. The diffuse reflectance spectra (Fig. S2†), transformed from reflectance to the Kubelka–Munk parameter $F(R)$, have generally sharper features than the solution phase UV-vis spectra. For **1–4**, two to three peaks noticeable below 25 000 cm^{-1}. The energies of the lowest-energy peaks increase in order from **2** (13 626 cm^{-1}) to **4** (13 633 cm^{-1}) to **3** (13 645 cm^{-1}) to **1** (14 004 cm^{-1}) in the solid-state, but are generally close in energy, like the solution-phase UV-vis data. This general similarity leads us to conclude there are no large differences structurally from compound to compound in solution, at least with respect to the CoO_6 coordination shell. However, the lowest-energy peaks are also generally lower than solution-phase values. This distinction, and other differences in the data, suggests the possibility of small structural changes in the solution phase, though we note the colors of the compounds in the solid state and the solutions are strikingly similar (Fig. S2†), suggesting a lack of gross changes to coordination geometry/structure/oxidation state, consistent with the general chemical stabilities of low-spin Co(III) ion bound by chelating ligands.[36]

Variable-temperature, solvent, and concentration [59]Co NMR analyses. We collected variable-temperature [59]Co NMR spectra to determine the temperature sensitivity of the [59]Co nuclei in **1–4**. Spectra were first collected on 10 mM solutions in $CDCl_3$ from 5 to 35 °C in the 11.74 T magnet of a 500 MHz (^{1}H) NMR (see Fig. S3–S6†). With increasing temperature, the [59]Co peaks for all complexes shift downfield to higher δ. Linear regression of the temperature dependence of the [59]Co chemical shifts yields the values of 2.71(1), 2.67(2), 1.55(4), and 2.78(2) ppm $°C^{-1}$ for **1–4**, respectively. We note that prior variable-temperature [59]Co NMR analysis of **4** set the prior record for $\Delta\delta/\Delta T$ for [59]Co NMR in air-stable Co(III) complexes at 3.15 ppm $°C^{-1}$. But, that original set was recorded at 3.52 T with a 100 mM solution in $CDCl_3$. We further note that Kanakubo later reported[37] a $\Delta\delta/\Delta T$ for **4** in $CHCl_3$ as 2.79(2) ppm, which aligns with our findings.

We tested the matrix sensitivity of the [59]Co thermal responses of **1–4** through variable-solvent (see Tables S3–S7†) and variable-concentration studies (see Tables S13, S14 and Fig. S8, S12, S16 and S25†). We selected a variety of solvents: $CHCl_3$, CH_2Cl_2, CD_2Cl_2, MeOH, DMSO and 1,2,4-trichlorobenzene (TCB), based on variance in physical properties such as polarity (from 2.2 to 47 for solvent TCB and DMSO, respectively) and viscosity (from 0.43 cP for CH_2Cl_2 to 32.9 cP for TCB).[38] Notably, **1–4** are not water-soluble and, hence, were not tested in aqueous solutions. The [59]Co NMR peak and its temperature sensitivity differed in each solvent (see Table S2†). The highest [59]Co $\Delta\delta/\Delta T$ values were observed for **1, 2-I, 2-II**,

and **4** in CDCl$_3$, 2.71(1), 2.69(1), 2.64(2), and 2.78(1) ppm °C^{-1} and **3**, 2.00(3) ppm °C^{-1}, in MeOH (see Tables S3–S7 and Fig. S7, S11, S15, S19 and S22†). Among these, the sensitivity of **3** was found to be the lowest of **1**–**4** in each solvent. In **2**–**4**, only slight changes (*ca.* 0.4 ppm °C^{-1}) were observed in $\Delta\delta/\Delta T$ with deuteration and no effect for **1**.

The origin of the solvent sensitivity likely stems from an impact from the solvent cage, though it is unclear precisely how that mechanism functions. In Co(III) amine complexes, solvent dependence of $\Delta\delta/\Delta T$ has been suggested to result from hydrogen-bonding interaction with donor solvents.[39] In **1**–**4**, there are no hydrogen bonding possibilities, which precludes that interaction as one of importance for $\Delta\delta/\Delta T$. There are also no apparent direct relationships between $\Delta\delta/\Delta T$ and polarity or viscosity of the solvent (Fig. S28 and S29†). Finally, we recognize that the solvent dependence is counterintuitive on the basis of sterics because of the variation of the chemical shift of **3** with solvent, which is wider than **1**, **2**, and **4**. One might expect, given the steric congestion afforded by the *t*Bu functional groups, that **3** should have the weakest solvent dependence, yet it does not, in agreement with some previous observations by Kanakubo.[37]

Variable-temperature ^{59}Co NMR spectra were collected on **1**–**4** at 1, 10, and 100 mM, revealing changes in the chemical shift and its temperature sensitivity with concentration (Fig. 4

Fig. 4 (a) Variable-temperature ^{59}Co NMR for **1** in CDCl$_3$ at 100 mM concentration. (b) Peak positions for **1**–**4** as a function of temperature at 100 mM concentration in CDCl$_3$.

and Fig. S7, S11, S15†). The ^{59}Co peak for compounds **1**–**4** in a 100 mM solution exhibited a downfield shift in the range of approximately 1–3 ppm compared to a 1 mM solution. Notably, the value of $\Delta\delta/\Delta T$ changed significantly, particularly for compound **1**, increasing to 3.50(2) °C^{-1}, at the increased concentration (Fig. 4). A similar trend is observed for **2**, where the $\Delta\delta/\Delta T$ value increased from 2.70(2) to 3.23(2) ppm °C^{-1} for **2-I**, and from 2.64(2) to 3.26(4) ppm °C^{-1} for **2-II**. Similarly, the $\Delta\delta/\Delta T$ value increased from 1.55(4) to 1.63(3) ppm °C^{-1} for **3**. Lastly, in **4** the ^{59}Co peak position appears significantly less dependent on concentration; only a small increase was observed in the sensitivity, from 2.78(2) to 2.83(2) ppm °C^{-1}. To the best of our knowledge, the observed value of 3.50 ppm °C^{-1} for **1** establishes a record for temperature sensitivity not only among closed-shell Co(III) complexes, but for all closed-shell species.

The origin of the concentration dependence of $\Delta\delta/\Delta T$ needs further investigation. It is reasonable to propose aggregation effects enhance the temperature sensitivity on account of the observed concentration dependence. However, there is no clear chemical difference in **1**–**4** that presents the possibility of aggregation in an intuitive way, *e.g.* functional groups for hydrogen bonding or open coordination sites. Furthermore, if such interactions exist, they are likely not magnetic in nature because they would be too weak. For instance, the dipole–dipole interaction between two ^{59}Co nuclei held at 7.47(1) Å apart (from the structure of **1**, the closest Co⋯Co distance in the crystal structures of **1**–**4** and likely closest possible distance in solution) is calculated to be only *ca.* 0.3 Hz (~6 ppm), significantly smaller than the total ranges observed (*ca.* 80 ppm, see Fig. 4). An alternative explanation of the concentration dependence is that aggregation is modifying how the individual ^{59}Co nuclei interact with the solvent cage. Changes in this interaction may induce changes in the electric field gradient at the cobalt nucleus,[40–43] which might also contribute to the concentration dependence of the chemical shift. Dynamic light scattering experiments as a function of concentration and solvent suggest that some degree of aggregation may be happening (see ESI†), though these changes do not trend with $\Delta\delta/\Delta T$, or any other magnetic resonance characteristic, across all studied concentrations and solvent choice. Note, finally, that the test of viscosity dependence of $\Delta\delta/\Delta T$ through the variable-solvent studies appears to disprove a mechanism stemming directly from increased viscosity of the higher-concentration solvents, or simply slower molecular motion in solution from aggregation.

Vibrational analyses. We anticipated that a descent in symmetry in the coordination environment would amplify the number of low-energy Raman-active modes in the complex, and therefore increase $\Delta\delta/\Delta T$. Hence, we applied Raman spectroscopy to evaluate the effect of the descending ligand symmetry on the vibrational spectra of **1**–**4** (Fig. 5). The selected spectral window (<650 cm^{-1}) targets vibrations that are appreciably populated at room temperature and the expected energy range of Co–L vibrations. As the probed molecules decrease in symmetry, the Raman spectra increase in complex-
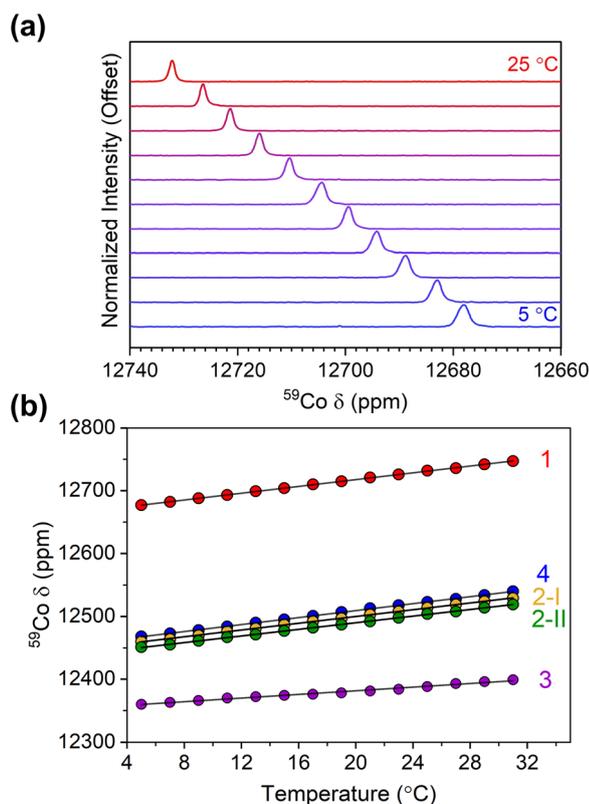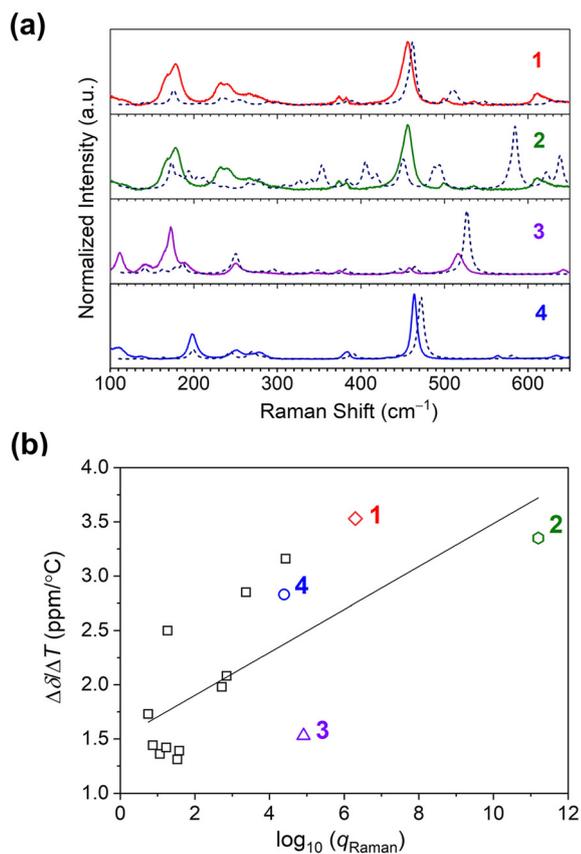
This journal is © the Partner Organisations 2023

Inorg. Chem. Front., 2023, **10**, 7064–7072 | **7067**

(a)

(b)

Fig. 5 (a) Room-temperature Raman spectra collected on microcrystalline samples of **1–4**. All spectra are baseline corrected. The dotted lines indicate the calculated spectra for the complexes. (b) The relationship between the ^{59}Co temperature sensitivity ($\Delta\delta/\Delta T$) and total vibrational partition function of Raman modes, q_{Raman}, for **1–4** (colored data points), and other Co(III) complexes (square data points). The linear correlation by R^2 is 0.49. Data for the other complexes are taken from ref. 15.

ity: asymmetric **1** and **2** display 12 and 17 bands below 650 cm^{-1}, respectively, whereas symmetric **3** and **4** exhibit 9 and 10 bands respectively. An exact correlation between the observed numbers of peaks and the simple group-theory analysis in the introduction (Fig. 1) does not occur. We suspect that this imperfect correlation is due to **1–4** having far more atoms than the local CoO$_6$ moiety and that there are potentially different isomers in **1** and **2**. Note, however, that the crystal structure of **1** seems to indicate only a single *mer* isomer, while the crystallographic data for **2** suggest that both *fac* and *mer* isomers are present. Hence, for **2** some of the additional peaks may stem from different isomers, whereas for **1** new peak (relative to **4**) are likely attributable to the descent in symmetry and splitting of *E*-symmetry Raman modes. There are additional considerations described further below.

Computational analysis of the vibrational spectra enabled assignment of the observed modes in the Raman spectra and comparison with $\Delta\delta/\Delta T$. The experimental spectra match the predicted spectra closely (see Fig. 5a). Experimentally, the most intense modes in all species are symmetric Co–O bond

stretching modes ("breathing" modes). These modes are observed at 456 cm^{-1} for **1**, and in the region of 563–568 cm^{-1} for **2**. For the symmetric complexes, this band is observed at 517 and 463 cm^{-1} for **3** and **4**, respectively. Bands below 200 cm^{-1} are mainly related to torsional modes of methyl or alkyl groups and the chelating ring.[44]
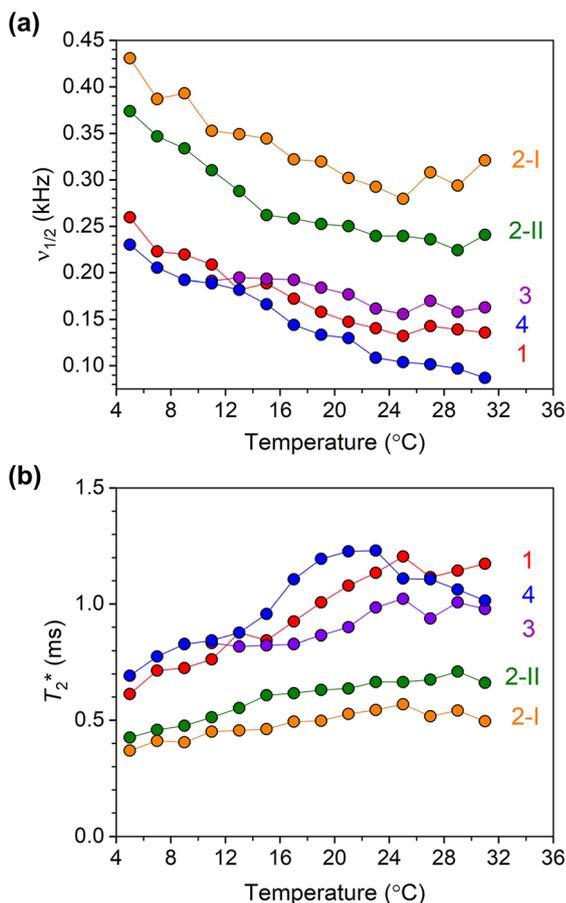
Role of ligand asymmetry in ^{59}Co $\Delta\delta/\Delta T$. We compared $\Delta\delta/\Delta T$ to the vibrational partition functions, q_{Raman}‡ of **1–4** using the computed vibrations from the frequency calculations concerning only the Raman active modes (see ESI for the calculation details and Tables S8–S11†). We compared these values against the aggregate of q_{Raman} v. $\Delta\delta/\Delta T$ data compiled in previous works[23,45] (Fig. 5). In general, the higher q_{Raman} values trend with higher $\Delta\delta/\Delta T$. Together, the comparison therefore suggests that a model for predicting temperature sensitivity based on a higher density of low-energy Raman vibrations is mostly correct, and that a ligand-asymmetry design strategy is one way to enhance $\Delta\delta/\Delta T$ through that model.

However, we note that the observed correlation between q_{Raman} and $\Delta\delta/\Delta T$ is weak, as indicated by the low correlation coefficient ($R^2 = 0.49$), and suggests the opportunity for significant future insight. We propose three important initial hypotheses behind the weak correlation for future study. First, we propose the need to factor in the extent to which a vibration is focused on the inner coordination shell into the partition function analyses. One may surmise a ligand-only vibration should have little impact on the ^{59}Co δ *versus* a Co–O-based mode, but that intuition needs quantitative testing, which could be available by local mode analyses.[46] Second, we propose that couplings between the solvent cage (or bulk solvent) and individual vibrational modes also need to be investigated in detail, because these interactions may ultimately alter which modes should be weighted for temperature sensitivity. This latter point may ultimately explain the concentration dependence if aggregation affects the couplings between specific vibrations and the solvent cage. Finally, third, we propose that understanding the exact physical structure of the species in solution is important, as the diffuse reflectance suggests some small alteration of the coordination shell. Such dynamic structural changes likely affect the vibrational spectra, and how this relates to the temperature sensitivity is a key future target.

^{59}Co NMR linewidth analyses. As one final experimental characterization, we performed linewidth analyses of the observed ^{59}Co peaks for **1–4** in all solvents and as a function of temperature (Fig. 6a). The linewidths ultimately help us describe the thermometer resolution (see below). The ^{59}Co NMR peaks for **1–4** in CDCl$_3$ at 25 °C all exhibit relatively sharp peaks with full width at half maximum values ($v_{1/2}$) of 1.12, 2.37, 1.38, and 0.85 ppm, respectively. These already narrow linewidths sharpen further with increasing tempera-

---

‡ q_{Raman} values are calculated from the product of each normal mode by

$$q_{Raman} = \prod_n \left(\frac{1}{1 - e^{-E_n/k_B T}} \right)$$ where E_n is the energy of the nth normal mode

(cm^{-1}), k_B is Boltzmann's constant, and T is the temperature (K).

7068 | *Inorg. Chem. Front.*, 2023, **10**, 7064–7072

This journal is © the Partner Organisations 2023

Fig. 6 (a) ^{59}Co NMR linewidth values for 10 mM solutions of **1–4** in CDCl$_3$ as a function of temperature. (b) Temperature dependence of T_2^* values for **1–4**, calculated using ^{59}Co NMR peak linewidths.

ture for **1–4** (Fig. 6a). In all complexes, only slight changes (*ca.* ~0.1 ppm in magnitude) were observed in linewidth with solvent (see Fig. S9, S13, S17, S20 and S23†), but in general, the narrowest peaks were observed in CH$_2$Cl$_2$, CDCl$_3$, and MeOH. Finally, for **2**, the linewidth of isomer **I** is found to be slightly broader than isomer **II** in all measured solvents. In all complexes, the broadest ^{59}Co NMR peaks are observed in DMSO.

The ^{59}Co NMR linewidths contain information about the relaxation time T_2^*, the dephasing time of the nuclear spin (analogous to the coherence time, T_2). The values of T_2^* were extracted from the temperature-dependent NMR linewidths through the relationship $T_2^* = 1/(2\pi\nu_{1/2})$ where $\nu_{1/2}$ (kHz) is the linewidth (at FWHM) of the ^{59}Co NMR peak. The temperature-dependent trends in T_2^* for all complexes over the 5–30 °C range are shown in Fig. 6b (see also Fig. S10, S14, S18, S21, and S24†) Complexes **1–4** all show generally increasing T_2^* with increasing temperature, where the temperature dependence is stronger for **1**, **3** and **4** than both isomers of **2**. Among all four complexes, **1** and **4** show the longest values of T_2^*. For both **1** and **4**, the longest T_2^* values are found in MeOH; 1.2 and 1.6 ms for **1** and **4**, respectively. While deuteration

increases T_2^* in CDCl$_3$ for **1**, only a small effect on T_2^* was observed in CD$_2$Cl$_2$. On the other hand, an increase in T_2^* in **4** upon deuteration was observed. For both isomers of **2**, T_2^* values are found to be similar. In all complexes, except **2-II** and **3** where the latter is insoluble, noticeably shorter T_2^* values are observed in DMSO. The T_2^* values were also found to decrease for all four complexes as the concentration increased from 10 mM to 100 mM. We also measured the spin–spin relaxations (T_2) for **1–4** *via* Carr–Purcell–Meiboom–Gill ("CPMG") experiments at room temperature (Fig. S26†). The T_2 values are 2.38(3), 0.99(2), 1.98(3) and 3.47(4) ms for **1–4**, respectively, all generally higher than the T_2^* values observed, but only a factor of 2. The T_2^* value is only determined for isomer **2-II** due to limitations in the data collections for **2-I**.

The T_2^* value of a quadrupolar nucleus like ^{59}Co is often dictated by spin–lattice relaxation (T_1), if T_1 is short enough that it limits the magnitude of T_2^*. We measured T_1 relaxation times *via* inversion recovery of **1–4** at room temperature (295 K) in 100 mM CDCl$_3$ solution (Fig. S27†). The T_1 values are 4.15(4), 1.23(2), 1.10(2), 2.24(3) and 4.01(4) ms for **1–4**, respectively, all on the order of the T_2 values obtained from CPMG and T_2^* from simple linewidth analyses. The effects of the T_1 times are observed in the ^{59}Co peak linewidths. Complexes **1** and **4**, with the longest T_1 values, have the narrowest ^{59}Co NMR peaks, whereas **2** and **3** exhibit shorter T_1 times. Hence, the linewidths here appear to follow spin–lattice relaxation times for the ^{59}Co nuclei in **1–4**.

There is additional importance of the linewidths and relaxation times in the context of the concentration dependence. Aggregation should be expected to slow down molecular rotation, potentially inducing larger linewidths through lengthening the correlation time.[47] If true, then the measured T_1 values would shorten, as would T_2, and all spectra would increase in linewidth with the increased aggregation observed from the DLS measurements. That we do *not* see these trends for relaxation time measurements from 1 to 100 mM concentrations (see Table S12† for DLS results and Tables S13 and S14 for variable-concentration relaxation data) suggests that whatever the nature of the observed aggregation, it is not having conventional impacts on the ^{59}Co NMR characteristics. Further, expecting the T_1 and T_2 data to follow the aggregation through correlation time variation does not acknowledge the substantial quadrupolar coupling for ^{59}Co, which is important for spin relaxation of this nucleus.[48–50] If aggregation were noticeably distorting the structure of the molecules, then these two competing systems ensure this system is far from trivial. Understanding these effects is key to sharper linewidths in future systems, and hence a key target for our future study.

^{59}Co NMR temperature sensing resolution. A key aspect of a sensor's utility is the resolution afforded in the sensing, which has not been described in the literature for ^{59}Co NMR systems to the best of our knowledge. We can parameterize this resolution through a ratio that compares the temperature sensitivity ($\Delta\delta/\Delta T$) with the full width half maximum of the peak ($\nu_{1/2}$): ($\Delta\delta/\Delta T)/\nu_{1/2}$. A higher ratio (in units of °C^{-1}) will enable

This journal is © the Partner Organisations 2023

Inorg. Chem. Front., 2023, **10**, 7064–7072 | **7069**

higher resolution of temperature sensing. The ratio points out an intuitive point: a sharp peak with high $\Delta\delta/\Delta T$ is advantageous for higher resolution thermometry.

We calculated the temperature resolution for **1–4** and contrasted them against values for other prominent NMR thermometer systems (Table 1). In complex **1**, the highest temperature sensitivity and the narrowest peak were observed in CDCl$_3$, which led to the ratio of 3.18, which is higher than Co(acac)$_3$ under the same conditions that we measured **1–4** in this paper. We also note that both isomers of complex **2** show lower resolution than **1** and **4** despite the high $\Delta\delta/\Delta T$, owing to the relatively wide linewidths of the two isomers. Among ^{59}Co NMR thermometers, these are the highest resolutions, eclipsing the recent spin-crossover ^{59}Co results.[20] They are also notably higher than the record temperature sensitivities for ^{1}H and ^{31}P. The sole measurement that eclipses our results in this manuscript is the original measurement of Co(acac)$_3$. Again, we stress the difference in the measurement technique as an essential part of the comparison, specifically the field of measurement which is likely affecting linewidth (11.7 T vs. ca. 3.2 T in the original Levy report). The resolution here is likely limited by the field of the measurement and the resolution for **1** would likely eclipse **4** if measured under the same conditions.

Conclusion

Tuning the number of allowed and forbidden IR and Raman-active modes in a molecule is a common exercise in inorganic and graduate level inorganic chemistry courses.[51] Here we show that applying the same course-work level analyses to conventional Co(III) complexes can yield new design strategies for $\Delta\delta/\Delta T$. Indeed, we present two new records for the temperature sensitivities of the ^{59}Co chemical shift in the asymmetric complexes Co(accp)$_3$ and Co(bzac)$_3$, the first in the over-40-year period since Co(acac)$_3$ was initially identified as an exciting NMR thermometer.[19]

While our study has predominantly focused on the design strategies to enhance temperature sensitivity in ^{59}Co NMR thermometry using air-stable Co(III) complexes, it is imperative to recognize that the translation of these findings into practical applications, particularly in biological or clinical settings, requires addressing issues related to toxicity and biocompatibility. Future investigations should explore encapsulation techniques and other strategies to increase stability and to mitigate potential toxicity concerns when applying these molecular thermometers in vivo.[52–55]

In a similar vein, it is important to note that new molecular imaging agents do not simply appear, but follow years of fundamental studies of magnetic properties in molecules.[52,56,57] It is in this context that this work should be appreciated for testing a new mechanism to increase temperature sensitivity in an ^{59}Co nucleus by molecular design. Yet, we acknowledge that further work is still necessary. For example, the trend in q_{Raman} with $\Delta\delta/\Delta T$ is not a perfect correlation, implying future experiments are needed, and while the measurements here focus on high-field analyses, conventional MRI is often performed at lower fields, suggesting low-field studies are also imperative. Finally, we need to understand what mechanisms are important for governing linewidth, as this knowledge could lead to higher resolution. Two parameters, quadrupolar coupling of the $I = {}^7/_2$ ^{59}Co nucleus and chemical shift anisotropy, are both proposed to dictate ^{59}Co NMR linewidth.[58] Studies of all of these effects will be reported in due course.

Author contributions

Ö. Ü. – methodology, investigation, formal analysis, validation, visualization, writing – original draft. S. S. – investigation, formal analysis. T. M. O – investigation, formal analysis. J. M. Z. – conceptualization, methodology, formal analysis, validation, funding acquisition, supervision, writing – review & editing.

Conflicts of interest

There are no conflicts to declare.

Table 1 Linewidths, $\nu_{1/2}$, and calculated temperature resolutions, $(\Delta\delta/\Delta T)/\nu_{1/2}$, for **1–4** and other notable NMR thermometers

Compound	$\nu_{1/2}{}^a$ (ppm)	$(\Delta\delta/\Delta T)/\nu_{1/2}$ (°C^{-1})
Co(acac)$_3{}^b$	0.86	3.66
Co(accp)$_3$ (**1**)^c	1.10	3.18
Co(bzac)$_3$ (**2**)^c	2.47	1.37
Co(tBu$_2$-acac)$_3$ (**3**)^c	1.34	1.22
Co(acac)$_3$ (**4**)^c	0.91	3.11
K$_3$[Co(CN)$_6$]^d	0.40	2.98
[Co(diNOsar)]Cl$_3{}^d$	12	0.17
[(CpCo(OP(OtBu)$_2$)$_3$)$_2$]Co^{+e}	128	1.18
^{1}H-[tBuPNPFe-H]^f	50	0.28
^{31}P-[tBu(PNP)Fe-H]^g	121	0.28

^{a} From room temperature values. ^{b} From original ref. 19 by Levy et al. ^{c} From this work. ^{d} Collected in H$_2$O at 33.3 mM concentration, 500 MHz magnet, see ref. 38. ^{e} Collected in CH$_2$Cl$_2$ at 400 mM, 500 MHz magnet, see ref. 20. ^{f} For ^{1}H NMR signal, from ref. 21. ^{g} For ^{31}P NMR signal, from ref. 22.

7070 | Inorg. Chem. Front., 2023, **10**, 7064–7072

This journal is © the Partner Organisations 2023

References

1 V. Ozenne, C. Constans, P. Bour, M. D. Santin, R. Valabregue, H. Ahnine, P. Pouget, S. Lehericy, J. F. Aubry and B. Quesson, MRI Monitoring of Temperature And Displacement For Transcranial Focus Ultrasound Applications, *Neuroimage*, 2020, **204**, 116236.

2 N. W. Lutz and M. Bernard, Contactless Thermometry by MRI and MRS: Advanced Methods for Thermotherapy and Biomaterials, *iScience*, 2020, **23**, 101561.

3 V. Rieke and K. Butts Pauly, MRI Thermometry, *J. Magn. Reson. Imaging*, 2008, **27**, 376–390.

4 N. M. Rzechorzek, M. J. Thrippleton, F. M. Chappell, G. Mair, A. Ercole, M. Cabeleira, C.-T. H. R. I. S.-S. Participants, Investigators, J. Rhodes, I. Marshall and J. S. O'Neill, A Daily Temperature Rhythm In The Human Brain Predicts Survival After Brain Injury, *Brain*, 2022, **145**, 2031–2048.

5 L. Brateman, Chemical Shift Imaging: A Review, *AJR, Am. J. Roentgenol.*, 1986, **146**, 971–980.

6 J. Blackwell, M. J. Krasny, A. O'Brien, K. Ashkan, J. Galligan, M. Destrade and N. Colgan, Proton Resonance Frequency Shift Thermometry: A Review of Modern Clinical Practices, *J. Magn. Reson. Imaging*, 2022, **55**, 389–403.

7 J. Yuan, C. S. Mei, L. P. Panych, N. J. McDannold and B. Madore, Towards Fast And Accurate Temperature Mapping With Proton Resonance Frequency-Based Mr Thermometry, *Quant. Imaging Med. Surg.*, 2012, **2**, 21–32.

8 C. Prinz, P. R. Delgado, T. W. Eigentler, L. Starke, T. Niendorf and S. Waiczies, Toward 19F Magnetic Resonance Thermometry: Spin-Lattice And Spin-Spin-Relaxation Times And Temperature Dependence of Fluorinated Drugs At 9.4 T, *MAGMA*, 2019, **32**, 51–61.

9 B. A. Berkowitz, J. T. Handa and C. A. Wilson, Perfluorocarbon Temperature Measurements Using ^{19}F NMR, *NMR Biomed.*, 1992, **5**, 65–68.

10 L. D. Field, S. Sternhell and W. Veigel, A High-Temperature Thermometer For ^{13}C NMR Spectroscopy, *Org. Magn. Reson.*, 1984, **22**, 221–223.

11 Y. Umegawa, Y. Tanaka, M. Nobuaki and M. Murata, 13C-Tmdota As Versatile Thermometer Compound For Solid-State NMR of Hydrated Lipid Bilayer Membranes, *Magn. Reson. Chem.*, 2016, **54**, 227–233.

12 F. L. Dickert and S. W. Hellmann, Chemical Shift Thermometer For Phosphorus-31 Nuclear Magnetic Resonance Measurements, *Anal. Chem.*, 2002, **52**, 996–996.

13 R. Estrada, N. Stolowich and M. C. Yappert, Influence of Temperature On 31P NMR Chemical Shifts of Phospholipids And Their Metabolites I. In Chloroform-Methanol-Water, *Anal. Biochem.*, 2008, **380**, 41–50.

14 G. Castro, G. Wang, T. Gambino, D. Esteban-Gomez, L. Valencia, G. Angelovski, C. Platas-Iglesias and P. Perez-Lourido, Lanthanide(III) Complexes Based on an 18-Membered Macrocycle Containing Acetamide Pendants. Structural Characterization and paraCEST Properties, *Inorg. Chem.*, 2021, **60**, 1902–1914.

15 S. Zhang, C. R. Malloy and A. D. Sherry, MRI Thermometry Based on PARACEST Agents, *J. Am. Chem. Soc.*, 2005, **127**, 17572–17573.

16 A. Yamasaki, Cobalt-59 Nuclear Magnetic Resonance Spectroscopy in Coordination Chemistry, *J. Coord. Chem.*, 1991, **24**, 211–260.

17 R. Bramley, M. Brorson, A. M. Sargeson and C. E. Schaeffer, Cobalt-59 NMR Chemical Shifts of Cobalt(III) Complexes: Correlations With Parameters Calculated From Ligand-Field Spectra, *J. Am. Chem. Soc.*, 2002, **107**, 2780–2787.

18 N. Juranić, A 59Co NMR Study of The Magnetic Shielding of The Cobalt Nucleus In Cobalt(III) Complexes, *J. Chem. Phys.*, 1981, **74**, 3690–3693.

19 G. C. Levy, J. Terry Bailey and D. A. Wright, A Sensitive NMR Thermometer For Multinuclei FT NMR, *J. Magn. Reson.*, 1980, **37**, 353–356.

20 O. Ungor, T. M. Ozvat, Z. Ni and J. M. Zadrozny, Record Chemical-Shift Temperature Sensitivity in a Series of Trinuclear Cobalt Complexes, *J. Am. Chem. Soc.*, 2022, **144**, 9132–9137.

21 J. C. Ott, H. Wadepohl, M. Enders and L. H. Gade, Taking Solution Proton NMR to Its Extreme: Prediction and Detection of a Hydride Resonance in an Intermediate-Spin Iron Complex, *J. Am. Chem. Soc.*, 2018, **140**, 17413–17417.

22 J. C. Ott, E. A. Suturina, I. Kuprov, J. Nehrkorn, A. Schnegg, M. Enders and L. H. Gade, Observability of Paramagnetic NMR Signals at over 10000 ppm Chemical Shifts, *Angew. Chem., Int. Ed.*, 2021, **60**, 22856–22864.

23 T. M. Ozvat, A. K. Rappe and J. M. Zadrozny, Isotopomeric Elucidation of the Mechanism of Temperature Sensitivity in 59Co NMR Molecular Thermometers, *Inorg. Chem.*, 2022, **61**, 778–785.

24 R. Liu, P. H. van Rooyen and J. Conradie, Geometrical Isomers of Tris(B-Diketonato)Metal(III) Complexes For M = Cr or Co: Synthesis, X-Ray Structures and DFT Study, *Inorg. Chim. Acta*, 2016, **447**, 59–65.

25 M. A. K. Ahmed, H. Flellvåg, A. Kjekshus and P. D. C. Dietzel, Syntheses, structures, and polymorphism of β-diketonato complexes -: Co(thd), *Z. Anorg. Allg. Chem.*, 2008, **634**, 247–254.

26 G. J. Krüger and E. C. Reynhardt, New Investigation of The Structure of Trisacetylacetonatocobalt(III), *Acta Crystallogr., Sect. B: Struct. Crystallogr. Cryst. Chem.*, 1974, **30**, 822–824.

27 S. Alvarez, D. Avnir, M. Llunell and M. Pinsky, Continuous Symmetry Maps And Shape Classification. The Case of Six-Coordinated Metal Compounds, *New J. Chem.*, 2002, **26**, 996–1009.

28 S. Alvarez, P. Alemany, D. Casanova, J. Cirera, M. Llunell and D. Avnir, Shape Maps and Polyhedral Interconversion Paths In Transition Metal Chemistry, *Coord. Chem. Rev.*, 2005, **249**, 1693–1708.

29 D. W. Barnum, Electronic Absorption Spectra of Acetyl-Acetonato Complexes-I, *J. Inorg. Nucl. Chem.*, 1961, **21**, 221–237.

30 E. N. Yurchenko, V. I. Avdeev and E. A. Shugam, Ultraviolet and Visible Absorption Spectra of Complexes of Trivalent

This journal is © the Partner Organisations 2023

Inorg. Chem. Front., 2023, **10**, 7064–7072 | 7071

Metals With Acetylacetonate and Its Analogs, *Theor. Exp. Chem.*, 1972, **6**, 73–77.

31 K. Kuroda, K. Yoshitani, K. Kunigita, Y. Kamiiba and K. Watanabe, Halogenation and Nitration of Some Mixed Ligand Acetylacetonato Cobalt(III) Complexes, *Bull. Chem. Soc. Jpn.*, 1976, **49**, 2445–2450.

32 J. T. Yarranton and J. K. McCusker, Ligand-Field Spectroscopy of Co(III) Complexes and the Development of a Spectrochemical Series for Low-Spin d(6) Charge-Transfer Chromophores, *J. Am. Chem. Soc.*, 2022, **144**, 12488–12500.

33 Y. Tanabe and S. Sugano, On the Absorption Spectra of Complex Ions II, *J. Phys. Soc. Jpn.*, 1954, **9**, 766–779.

34 S. C. F. Au-Yeung, K. W. Kwong and R. J. Buist, Multinuclear NMR Study of The Crystal Field Strength of The Nitro Ligand And The Empirical Estimation of The Cobalt-59 NMR Chemical Shifts of Cobalt-Nitro Complexes, *J. Am. Chem. Soc.*, 2002, **112**, 7482–7488.

35 M. Fujita, T. Fujihara, M. Kojima, Y. Yoshikawa and K. Yamasaki, Preparative Study and Characterization of the Cis-Diamminetetranitrocobaltate(III) Ion. A Missing Link in the Ammine-Nitro Cobalt(III) Series, *Proc. Jpn. Soc.*, 1997, **73**, 161–164.

36 B. Figgis and M. Hitchman, *Ligand field theory and its applications*, Wiley-VCH, New York, 2000.

37 M. Kanakubo, T. Uda, H. Ikeuchi and G. P. Satô, Solvent and Temperature Dependence of 59Co NMR Chemical Shifts of Tris(acetylacetonato)cobaIt(III) and Tris(dipivaloylmethanato)cobalt(III), *J. Solution Chem.*, 1998, **27**, 645–653.

38 J. A. Dean, *"Lange's Handbook of Chemistry"*, McGraw Hill Inc., New York, 1992.

39 T. M. Ozvat, M. E. Pena and J. M. Zadrozny, Influence of Ligand Encapsulation On Cobalt-59 Chemical-Shift Thermometry, *Chem. Sci.*, 2019, **10**, 6727–6734.

40 K. L. Craighead and R. G. Bryant, Insignificance of Second Coordination Sphere Interactions in Cobalt-59 Nuclear Magnetic Resonance Relaxation, *J. Phys. Chem.*, 2002, **79**, 1602–1603.

41 T. H. Martin and B. M. Fung, Outer Sphere Complex Between Trisethylenediaminecobalt(III) and Phosphate, *J. Phys. Chem.*, 2002, **77**, 637–640.

42 P. Zhou, S. C. F. Au-Yeung and X. P. Xu, A DFT And Co Solid-State NMR Study of The Second-Sphere Interaction In Polyammonium Macrocycles Cobalt Cyanide Supercomplexes, *J. Am. Chem. Soc.*, 1999, **121**, 1030–1036.

43 K. Rose and R. G. Bryant, The Insignificance of Second Coordination Sphere Interactions in Cobalt-59 NMR Relaxation: A More Precise Assessment, *J. Magn. Reson.*, 1979, **35**, 223–226.

44 H. Fakheri, S. F. Tayyari, M. M. Heravi and A. Morsali, Low Frequency Vibrational Spectra And The Nature of Metal-Oxygen Bond of Alkaline Earth Metal Acetylacetonates, *J. Mol. Struct.*, 2017, **1150**, 340–348.

45 C. J. Jameson, D. Rehder and M. Hoch, Isotope And Temperature Dependence Of Transition-Metal Shielding In Complexes Of The Type M(XY)6, *J. Am. Chem. Soc.*, 2002, **109**, 2589–2594.

46 E. Kraka, W. Zou and Y. Tao, Decoding Chemical Information From Vibrational Spectroscopy Data: Local Vibrational Mode Theory, *Wiley Interdiscip. Rev.: Comput. Mol. Sci.*, 2020, **10**, e1480.

47 M. H. Levitt, *Spin Dynamics*, John Wiley & Sons, Inc., New York, 2nd edn, 2008.

48 T. M. Ozvat, S. H. Johnson, A. K. Rappé and J. M. Zadrozny, Ligand Control of ^{59}Co Nuclear Spin Relaxation Thermometry, *Magnetochemistry*, 2020, **6**, 58–58.

49 D. M. Doddrell, M. R. Bendall, P. C. Healy, G. Smith, C. H. L. Kennard, C. L. Raston and A. H. White, 59Co and 13C Nuclear Spin Relaxation Studies in Solutions of Symmetric, Bidentate Cobalt(III) Complexes. On the Mechanism of 59Co Spin Relaxation. Crystal Structure Determination of Tris(tropolonato)cobalt(III), *Aust. J. Chem.*, 1979, **32**, 1219–1230.

50 S. C. F. F. Au-Yeung, R. J. Buist and D. R. Eaton, Spin-Lattice Relaxation in Co Complexes of Low Symmetry, *J. Magn. Reson.*, 1983, **55**, 24–38.

51 F. A. Cotton, *"Chemical Applications of Group Theory"*, Wiley-Interscience, New York, 3rd edn, 1990.

52 J. Wahsner, E. M. Gale, A. Rodriguez-Rodriguez and P. Caravan, Chemistry of MRI Contrast Agents: Current Challenges and New Frontiers, *Chem. Rev.*, 2019, **119**, 957–1057.

53 F. Schilling, L. Schroder, K. K. Palaniappan, S. Zapf, D. E. Wemmer and A. Pines, MRI Thermometry Based On Encapsulated Hyperpolarized Xenon, *Chem. Phys.*, 2010, **11**, 3529–3533.

54 G. H. Gao, G. H. Im, M. S. Kim, J. W. Lee, J. Yang, H. Jeon, J. H. Lee and D. S. Lee, Magnetite-Nanoparticle-Encapsulated pH-Responsive Polymeric Micelle As An MRI Probe For Detecting Acidic Pathologic Areas, *Small*, 2010, **6**, 1201–1204.

55 Y. Yang, D. T. Schuhle, G. Dai, J. K. Alford and P. Caravan, 1H Chemical Shift Magnetic Resonance Imaging Probes With High Sensitivity For Multiplex Imaging, *Contrast Media Mol. Imaging*, 2012, **7**, 276–279.

56 I. R. Young, Significant Events In The Development of MRI, *J. Magn. Reson. Imaging*, 2004, **20**, 183–186.

57 M. A. Sieber, T. Steger-Hartmann, P. Lengsfeld and H. Pietsch, Gadolinium-Based Contrast Agents And NSF: Evidence From Animal Experience, *J. Magn. Reson. Imaging*, 2009, **30**, 1268–1276.

58 A. Medek, V. Frydman and L. Frydman, Solid and Liquid Phase ^{59}Co NMR Studies of Cobalamins and Their Derivatives, *Proc. Natl. Acad. Sci. U. S. A.*, 1997, **94**, 14237–14242.

7072 | *Inorg. Chem. Front.*, 2023, **10**, 7064–7072

This journal is © the Partner Organisations 2023